Title
A system of methods to investigate brain metabolism of a mouse model using Hyperpolarized 13C

Author
Qiao, Kai Wen

Publication Date
2018

Peer reviewed|Thesis/dissertation

A system of methods to investigate brain metabolism of a mouse model using Hyperpolarized ^{13}C

by

Kai Wen Qiao

THESIS

Submitted in partial satisfaction of the requirements for the degree of

MASTER OF SCIENCE

in

Biomedical Imaging

in the

GRADUATE DIVISION

of the

UNIVERSITY OF CALIFORNIA, SAN FRANCISCO

To

Mom

&

Grandma

Acknowledgements

Lab collaborators

Chaumeil Lab

Kurhanewicz Lab

Ronen Lab

Swanson Lab

Thesis committee

Myriam Chaumeil, PhD

Peder Larson, PhD

Ken Nakamura, MD, PhD

Renuka Sriram, PhD

A system of methods to investigate brain metabolism of a mouse model using Hyperpolarized ^{13}C

Kai Wen Qiao

Brain metabolism studies have become increasingly popular as public awareness of the crucial role of metabolic impairment in neurodegenerative and neuroinflammatory diseases grows. With the current proliferation of hyperpolarized ^{13}C (HP ^{13}C) Magnetic Resonance Spectroscopy/Imaging (MRS/I) based on dissolution Dynamic Nuclear Polarization (dDNP), metabolic studies are in an exciting stage. Here a collection of three methods are aggregated, optimized, and presented as a general guideline for HP ^{13}C metabolic studies of the mouse model. Firstly, *in vivo* Magnetic Resonance Spectroscopy (MRS) was performed utilizing the innovative dDNP of HP [1-^{13}C] pyruvate. Five 12-week-old mice were imaged using a surface coil in a 3 Tesla preclinical system, with varying parameters such as time repetition (TR), flip angle, and pyruvate probe concentration. All spectra produced pyruvate and lactate peaks, and two acquisitions exhibited quantifiable bicarbonate peaks. The second, *ex vivo* component utilized a near-physiological NMR compatible perfusion system, which was optimized for maintaining viable fresh brain tissue slices. Viability was tested with an electrode measuring O_2 levels of media, with nonviable samples consuming little to no O_2. Over 7 hours of perfusion, all slices tested were compared to a negative control and deemed viable. Lastly, an enzyme activity assay is included as a robust validation tool. The 3 component system spans across multiple biological hierarchies, and each method balances the strengths and weaknesses of the other. Moving forward, HP ^{13}C studies of brain metabolism utilizing this system will produce clear, robust results that can be applied to nearly any mouse model.

Table of Contents

List of Tables

List of Figures

Prologue

Introduction

Brain metabolism

Metabolism is a collection of chemical processes that allow for biological function. In the brain, metabolic studies are becoming increasingly popular in large part due to increased awareness of the crucial role of metabolic impairment in neurodegenerative and neuroinflammatory diseases. Increased understanding of disorders such as Chronic Traumatic Encephalitis (CTE) and Alzheimer's disease (AD) has expanded research scope, and metabolomics is an increasingly promising field to add. To date, multiple studies have linked metabolic changes to diseases such as Hungtington's[1], Alzheimer's[2], Parkingson's[3], Schizophrenia[4], and even addiction[5]. Thus, a careful understanding of metabolism can lead to early diagnoses, disease progression mapping, and treatment development. Current studies of metabolism incorporate assays, proteomics, immunology, and gels[6], but a relatively recent development in the field of magnetic resonance spectroscopy (MRS) is gaining ground.

Hyperpolarized ^{13}C MRS, dissolution dynamic nuclear polarization, and relaxation time T1

Nuclear magnetic resonance (NMR) characterizes how the nuclei of an atom behaves in a magnetic field. A radiofrequency wave (RF) in the system excites the nuclei, producing a signal that's recorded as a free induction decay (FID)[7]. This FID can then be converted from the time domain into the frequency domain by Fourier transform, giving rise to an MR spectrum. Depending on its electron environment, the nuclei's behavior changes and is reflected as

frequency shifts in units of ppm. ^{13}C, an isotope of carbon, has been employed for decades to distinguish between organic compounds with a carbon backbone. The natural abundance of carbon ^{12}C is 98.9% and is MR invisible, while ^{13}C abundance is much lower at 1.1% but is MR visible due to its spin properties. Upon injection of a ^{13}C – enriched metabolite, the natural rarity of ^{13}C allows for clean, discernible spectra of the ^{13}C – labeled substrate and its metabolic products without nearly as much background signal as typical proton MRS[8]. Although ^{13}C signal is not contaminated with background signal, the gyromagnetic ratio of ^{13}C is 1/4th that of ^{1}H, resulting in low MR signal overall[9]. Some methods to allay the low signal issue include increased acquisition time[10] and proton decoupling[9,11], but a relatively new method of hyperpolarizing the ^{13}C with dissolution dynamic nuclear polarization[12] (dDNP) provides the best signal increase.

Currently, hyperpolarized ^{13}C (HP ^{13}C) enjoys an up to 50,000 – fold increase[13] in MR signal. To begin, a metabolite enriched for ^{13}C at desired positions on the carbon backbone is mixed homogeneously with a radical, typically OX063. This mixture is introduced into the magnet bore of a polarizer such as the commercial HyperSense (Oxford, UK) system, where a liquid helium pool cools the sample to less than 2 Kelvin. In a build-up time of roughly 1 hour, a microwave source induces the transfer of polarization from the radical to the ^{13}C on the metabolite[13]. The frozen, hyperpolarized mixture is then simultaneously heated, dissolved, and pH balanced for its ready-to-inject form.

The hyperpolarization of ^{13}C is short lived however, and is characterized by the spin-lattice relaxation time T1. Upon dissolution, the polarization signal decays exponentially with a time constant of T1. After one T1, only 37% of the hyperpolarized signal remains, and just 13.5% signal is leftover after two T1[13]. The T1 is highly dependent on the chemical structure of

the hyperpolarized compound, as well as the solvents used and the immediate resulting magnetic field during data acquisition. For example, the T1 of ^{13}C pyruvate labeled on the 1st carbon position ([1-^{13}C] pyruvate) ranges from 67 seconds at a magnetic field strength of 3 Tesla (T) to 44 seconds at 14.1T[14,15].

Pyruvate and the Krebs cycle

The Krebs cycle (or citric acid cycle, or TCA cycle) is a crucial metabolic pathway for aerobic living systems. A primary role of the Krebs cycle is to fuel the electron transport chain (ETC) with high energy electrons to allow for efficient generation of adenosine tri-phosphate (ATP)[16]. The cycle begins with shuttling the cytoplasmic pyruvate into the mitochondrial matrix followed by conversion to acetyl-CoA as seen in **Figure 1**. This conversion is achieved by the pyruvate dehydrogenase (PDH) enzyme complex[17], and CO_2 is released and observed in the form of bicarbonate through a rapid equilibrium catalyzed by carbonic anhydrase (CA). Another major path follows the conversion of pyruvate into lactate by the lactate dehydrogenase (LDH) enzyme. Lactate formation leads to a much less efficient means of ATP generation, though it does not require oxygen the way ETC does. Also, under pathological conditions such as cancer, numerous studies show an unmistakable bias towards the less efficient lactate pathway (a phenomenon referred to as the Warburg effect, or aerobic glycolysis)[18,19]. This unique situation places pyruvate at a crossroads between two distinctly different pathways, where its understanding provides an appreciable window into the metabolic health of a system.

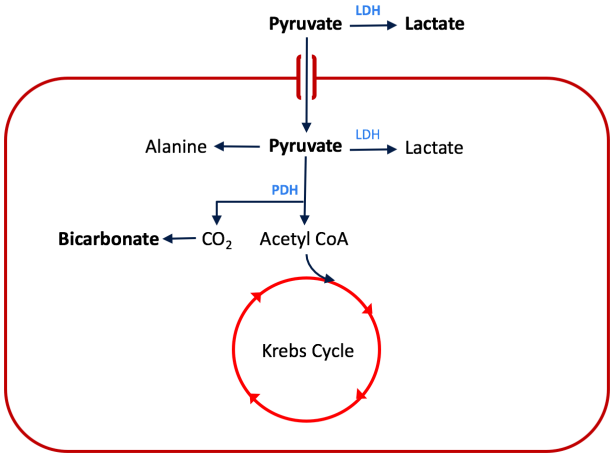

Figure 1. Illustration of cytoplasmic pyruvate shuttled into mitochondrial matrix, and metabolic fates of pyruvate. Larger fraction of lactate formed in cytosol than in matrix. Upon acetyl CoA formation, resulting CO2 is in immediate equilibrium with bicarbonate.

Not only is pyruvate uniquely in the center of major metabolic pathways, the chemical structure of pyruvate provides a rather stable platform for retaining ^{13}C polarization. The T1 of [1-^{13}C] pyruvate is upwards of 40 seconds in comparison to the 14 seconds of [2-^{13}C] fructose at 3T field strength[20]. The longer T1 allows for the hyperpolarized metabolite to not only reach the target, but to metabolize and produce spectroscopic data of the product metabolites making [1-^{13}C] pyruvate an ideal probe. For [1-^{13}C] pyruvate undergoing the PDH path, the ^{13}C on the first carbon position will be cleaved and results in labeled $^{13}CO_2$ described in **Figure 2a**. In physiological conditions, $^{13}CO_2$ will be in equilibrium with bicarbonate through CA catalysis. In the presence of water, $^{13}CO_2$ is quickly hydrated into carbonic acid and subsequently neutralized into bicarbonate[16]. Thus, at physiological pH, the labeled metabolic product to be observed in the spectra is bicarbonate. Following [1-^{13}C] pyruvate through the LDH path, the ^{13}C remains in the lactate structure seen in **Figure 2b**, and consequently lactate is the metabolic product to detect. By probing for differences in metabolite quantities and product formation rates, pathologies can be characterized with metabolic imaging.

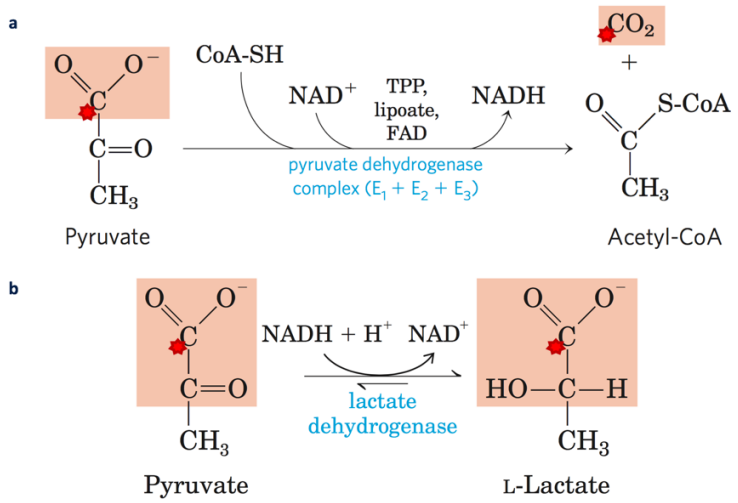

Figure 2. Two major pathways of pyruvate metabolism. (a) Conversion of pyruvate to acetyl-CoA by PDH enzyme and complex. The ^{13}C on the first position of [1-^{13}C] pyruvate (hyperpolarized ^{13}C represented by the star) results in $^{13}CO_2$, and is in equilibrium with bicarbonate. (b) Pyruvate is reduced to lactate by LDH enzyme, and the ^{13}C label is conserved in the lactate structure. From Lehninger Principles of Biochemistry (p. 541-634), Nelson DL, Cox MM, 2013, New York: W. H. Freeman and Company. Copyright 2013 by W. H. Freeman and Company.

Hyperpolarized ^{13}C studies and project motive

To date, multiple studies involving hyperpolarized ^{13}C MRS have been documented. Some *in vivo* applications include assessing diabetic hearts in mice[21], human glioblastoma xenografts in rats[22], and the first clinical trial investigating prostate cancer[23]. *Ex vivo* studies have been performed on U87 cancer cells[24], and hyperpolarized ^{13}C data have been linked to changes in activities of LDH and PDH[13].

This project's goal is to create a cohesive HP ^{13}C brain metabolism study, which is realized by combining three components: *In vivo* MRS, *ex vivo* MRS, and direct enzyme activity data. By combining the three classes, *in vivo* data can be correlated with the *ex vivo* findings, and both results can be validated by enzyme activity assays – the current gold standard for studying metabolism. The three classes together also progressively increase in biological hierarchy, forming a robust and cohesive system for any study.

Chapter 1

In vivo hyperpolarized ^{13}C MR spectroscopy

Introduction

Typically, *in vivo* imaging studies are the most translatable to clinical practice. Many studies involving molecular imaging use mouse models to identify suitable biological targets before employing them in the clinic[25]. Optical imaging of tracers and sonography have been used in preclinical studies with high impact in the clinic as well[26]. Keeping in mind the goal to bring HP ^{13}C MRS into the clinic, *in vivo* studies are critical and therefore motive to include in this system of methods. A major goal of this *in vivo* HP ^{13}C MRS experiment was to observe the lactate and bicarbonate metabolites. Since bicarbonate is produced further down from initial pyruvate processing, its signal is naturally lower and more difficult to detect. Some methods to maximize signal includes a non-localized pulse sequence to receive signal from the entirety of the coil's sensitivity profile, as well as summing all spectra from a dynamic acquisition.

Materials and methods

Animal and preparation

Five 12-week-old female C57BL/6J strain control mice (Jackson Laboratories) were used for five *in vivo* imaging acquisitions. 1.5% Isoflurane and O_2 mixture was administered and a negative pedal pain reflex was obtained before catheterization. A catheter was placed in the tail vein and a 0.9% saline USP solution was used. The catheter was 100cm long, and ~300μL of the

hyperpolarized [1-^{13}C] pyruvate mixture was injected over 20 seconds. All handling practices were in accordance with University of California, San Francisco IACUC approved guidelines.

Chemicals and ^{13}C probe

Two concentrations of [1-^{13}C] pyruvate were used (24uL in 4.5mL solvent, and 48uL in 4.5mL solvent). 80mM mouse buffer containing 80mM NaOH, 40mM Tris, and 0.3mM EDTA was used as a solvent for dissolution and pH balance of the lower pyruvate concentration. 160mM mouse buffer containing 160mM NaOH, 80mM Tris, and 0.6mM EDTA was used for the higher [1-^{13}C] pyruvate concentration. The concentrations used and corresponding acquisitions are summarized in **Table 1**. All mixtures injected into mice were room temperature with pH of 7. The OX063 radical was used to hyperpolarize the pyruvate sample, utilizing the HyperSense with a magnetic field strength of 3.35T and a typical polarized sample temperature of ~1.5K.

MR equipment

The preclinical BioSpec 3T (Bruker) system was used to acquire ^{13}C spectroscopy. A mouse bed was used to stabilize the in-house developed cranial surface coil. The surface coil contained two ^{1}H coils, one on each side of the mouse head, and a single ^{13}C coil directly above cranial isocenter as seen in **Figure 3.** A 6M urea phantom was placed above the head in two acquisitions, and the remaining three acquisitions used a phantom containing 5M of ^{13}C- HMCP (hydroxymethyl cyclopropane), subsequently referred to as HP001[27].

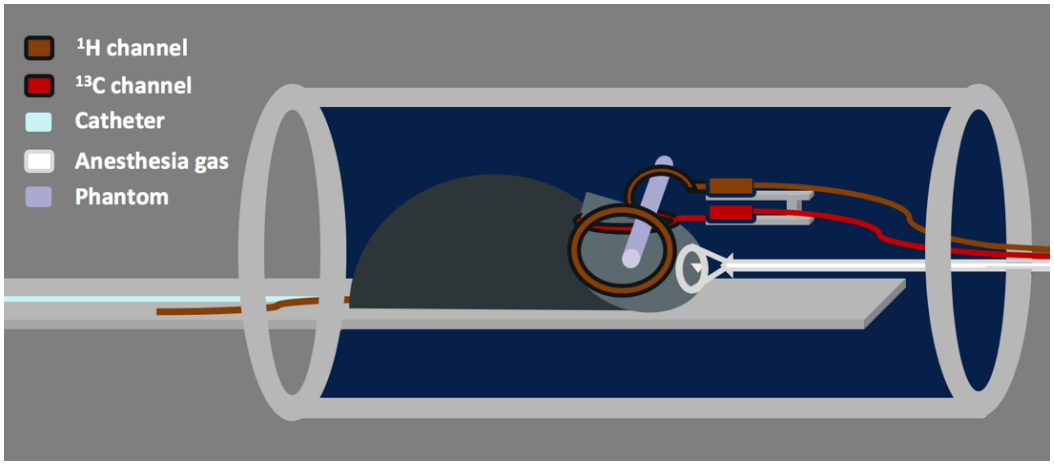

Figure 3. *In vivo* setup with surface coil orientation in the 3T MR system. Single ^{13}C coil in red and dual ^{1}H coils on either side of skull, with the phantom positioned across. Isoflurane and O_2 mixture delivered to nose cone, and catheter placed in the tail vein.

MR parameters

A non-localized pulse acquire sequence was used to record the entire field of view of the ^{13}C coil. Different repetition times (TR), flip angles, and shim results of the five acquisitions are detailed in **Table 1.** The bandwidth was set at 40ppm and centered at 163ppm.

Acq.	[1-^{13}C] Pyr	Buffer	Phantom	TR	Flip	Shim
1	24μL	80mM	Urea	3s	15°	24Hz
2	24μL	80mM	Urea	3s	25°	16Hz
3	24μL	80mM	HP001	3s	10°	14Hz
4	48μL	160mM	HP001	4s	10°	15.6Hz
5	48μL	160mM	HP001	4s	10°	12.2Hz

Table 1. Some MR parameters of the five *in vivo* acquisitions. Volume of pyruvate probe includes the homogenously mixed OX063 radical and 4.5mL of buffer solvent. Full width half maximum shim reported.

Processing and analysis

FID and spectra processing and analysis were accomplished with jMRUI[28] version 4.0 build 113. All FIDs had the first 68 points truncated due to an inherent property of Bruker

systems starting FID recording before the actual start of acquisition. A 5Hz Lorentzian apodization was applied to every spectrum, and the summation spectra was produced by summing the entire dynamic acquisition. Peak amplitudes of sum spectra were calculated using the AMARES[29] algorithm in jMRUI.

Results

Decent spectral resolution was achieved overall, and the 3rd acquisition's signal to noise ratio (SNR) was the highest among the five scans. Acquisition 3's dynamic HP ^{13}C spectra and sum are demonstrated in **Figure 4.** Alanine and bicarbonate peaks of the other four acquisitions were either absent or below noise floor. The AMARES quantitation of acquisition 4 does find bicarbonate however. **Table 2** reports the quantifiable peak amplitudes and lactate/pyruvate ratio for all acquisition sums.

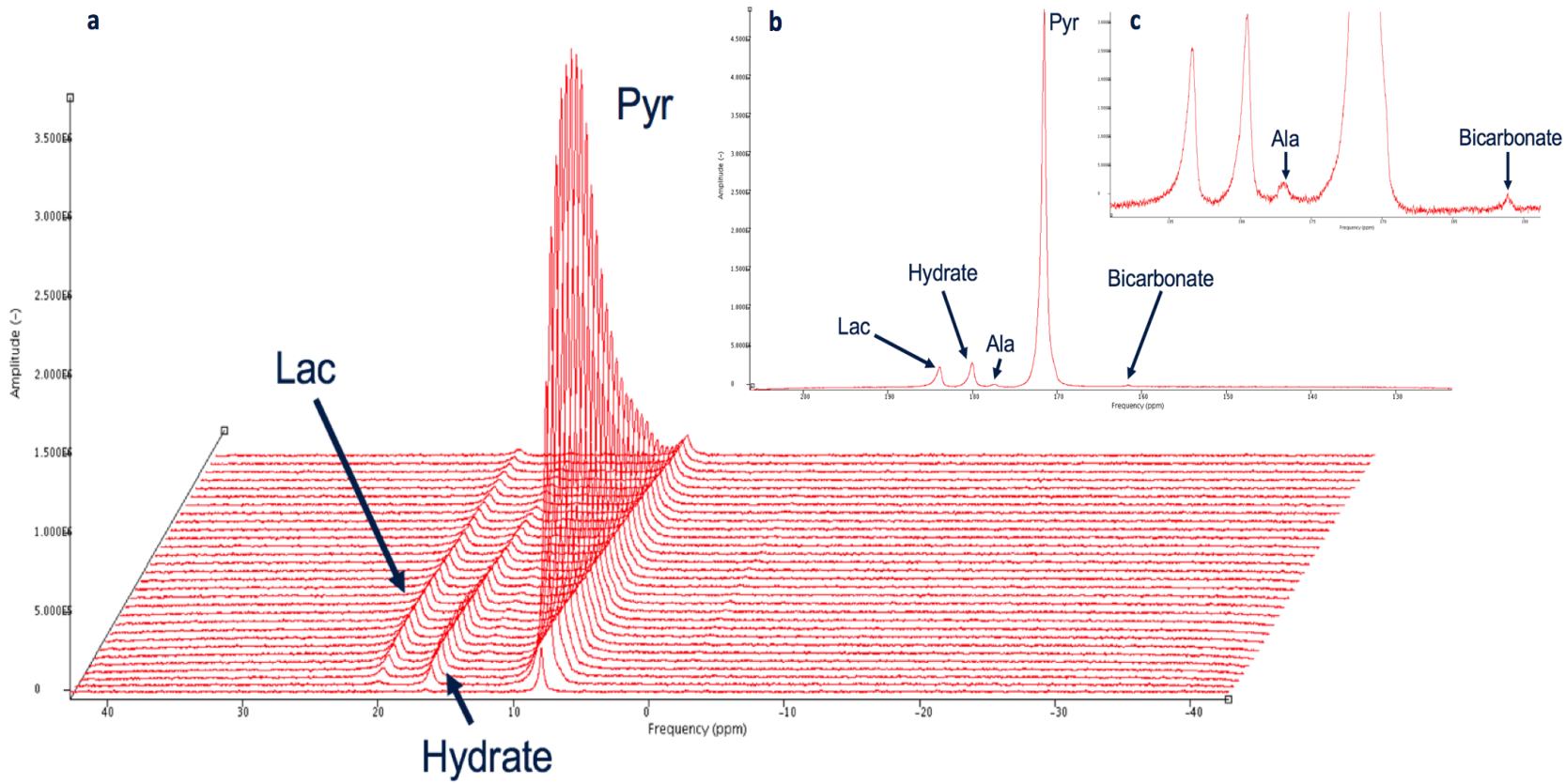

Figure 4. ^{13}C MRS spectra following [1-^{13}C] pyruvate injection. (a) Dynamic spectra with smooth pyruvate accumulation and wash out signal, as well as clearly visible lactate and pyruvate hydrate signals. (b) Summation of total dynamic acquisition into single spectra and (c) zoomed view to distinguish alanine and bicarbonate peaks.

Acq.	Lactate	Hydrate	Alanine	Pyruvate	Bicarbonate	Lac/Pyr
1	$6.46 \cdot 10^3$	$1.93 \cdot 10^3$	-	$2.83 \cdot 10^4$	-	$2.29 \cdot 10^{-1}$
2	$1.14 \cdot 10^4$	$7.95 \cdot 10^3$	$1.27 \cdot 10^3$	$1.10 \cdot 10^5$	-	$1.03 \cdot 10^{-1}$
3	$6.71 \cdot 10^4$	$7.73 \cdot 10^4$	$4.11 \cdot 10^3$	$1.09 \cdot 10^6$	$8.32 \cdot 10^3$	$6.16 \cdot 10^{-2}$
4	$1.11 \cdot 10^4$	$2.09 \cdot 10^4$	-	$6.58 \cdot 10^5$	$2.59 \cdot 10^3$*	$1.69 \cdot 10^{-2}$
5	$4.80 \cdot 10^3$	$6.43 \cdot 10^3$	-	$1.71 \cdot 10^5$	-	$2.82 \cdot 10^{-2}$

Table 2. Metabolite peak amplitudes for each acquisition. Absent peaks from spectral data left blank, and bicarbonate quantitation of acquisition 4 included although peak was difficult to discern due to slightly poor spectral resolution. Acquisitions 4 and 5 had twice the concentration of ^{13}C probe injected compared to that of acquisitions 1-3.

Discussion

HP ^{13}C probe concentration

The desired outcome of this *in vivo* HP ^{13}C MRS experiment was to observe the lactate and bicarbonate metabolites. It was postulated that overall a higher signal across the board would be observed if the initial injected concentration of [1-^{13}C] pyruvate was doubled. This was not the case however, as even the peak amplitudes of pyruvate were lower in acqs. 4 and 5 compared to acq. 3. This could either simply be an inadequate delivery to the brain in those mice, or a much more convoluted mechanism is at play. It should be noted that a higher pyruvate signal does correspond with successful bicarbonate quantification, suggesting that the MR parameters of acqs. 3 and 4 are adequate and future studies need only to increase polarization signal. This is extremely limited data however, and many more in vivo acquisitions with similar parameters are needed to confirm. The high variability of lactate/pyruvate ratios between acquisitions should be noted, and further investigation is required. Also, only the peak amplitudes were considered, and peaks areas should've been more appropriate since different shims were used across the acquisitions.

Phantom choice

The phantom is an important aspect of *in* vivo spectroscopy. The signal from the phantom could be compared across acquisitions to monitor consistency of acquisition parameters, and be used for normalization. For instance, had the phantom signals of acqs. 4 and 5 remained consistent with acq. 3, the lower pyruvate signals can be confidently attributed to poor metabolite delivery. Inconsistent phantom signals would suggest hardware or acquisition parameter issues, and the results would not be directly comparable. For acquisitions 1 and 2, a urea phantom was used to center the spectral acquisition window on a known, visible signal. This was a mistake however, as the chemical shift of bicarbonate is just upfield of urea. Because the urea phantom is placed next to – and not in – the brain, and that the gradient shimming targeted solely the brain, the spectral resolution of urea suffered heavily and cannibalized all the small peaks nearby. When the urea phantom was switched out for HP001, a phantom with a chemical shift far outside the window of interest, a clean bicarbonate signal was observed in acq. 3. HP001 still isn't the optimal phantom however, as its δ = 70ppm chemical shift[27] is outside of the prescribed 40ppm bandwidth. To observe the phantom's signal, bandwidth must be increased, but doing so compromises spectral resolution. Since bicarbonate signal was desired, the choice was to preserve spectral resolution and forego the phantom. Future work includes testing larger bandwidths, as well as phantoms with more optimal chemical shifts.

Non-localized pulse acquire sequence

Although lactate and bicarbonate peaks were observed, the use of non-localized pulse sequences are impractical for clinical diagnostic imaging, and the furthest from precision medicine. The pulse acquire sequence grabs signal from the entire field of view of the ^{13}C coil, including the surrounding spaces that are not brain. Although only ^{13}C labeled metabolites are detected, the resulting spectra is a collective of intracellular and extracellular data. The current sensitivity of the surface coil is barely able to pick up bicarbonate signal with a pulse acquire sequence, and likely insensitive to bicarbonate with a more targeted sequence. Future work includes increasing sensitivity by addition of a second ^{13}C coil, or implementing more advanced sequences such as spectral – selective excitation pulses[30].

The overall *in vivo* experimental design performed here still requires refinement. Finding comparable studies is challenging, as values are typically reported in peak areas, and pulse acquire sequences of the brain are not common. A study using a pulse acquire sequence with reported bicarbonate signal needed to increase flip angle from 4.5 degrees to 43 degrees[31], a drastic difference from the 10 degrees used here. It should be noted that their TR was incredibly short at 0.75 seconds however, limiting their relaxation and consequently reducing signal. *In vivo* lactate/pyruvate ratios of the brain using localized pulse sequences are consistently reported though, with values between 5-15 percent[32]. This is comparable to acq. 3's 6 percent, but the pulse sequences are completely different and values are still peak area vs. peak amplitude. Future work includes more HP ^{13}C MRS with acq. 3's parameters, analyzing for peak areas, and testing bandwidths that accommodate phantoms without too much spectral resolution compromise

Chapter 2

Ex vivo NMR compatible perfusion system

Introduction

Issues with in vivo HP ^{13}C MRS

Although *in vivo* imaging studies are the most translatable to the clinic, there are some factors to consider in the context of HP ^{13}C MRS. Because the ^{13}C metabolite is introduced intravenously, the rate of metabolite delivery to the target of interest must be considered. Factors such as the physical blood brain barrier (BBB) or cardiovascular disease can inhibit delivery of the ^{13}C probe, erroneously producing a "reduced" metabolism reading at the target of interest. Other factors such as wash-in and wash-out of metabolites from neighboring organs can confound the data. Thus, to probe absolute metabolic rates with HP ^{13}C MRS, *ex vivo* studies on tissue slices can be a promising solution. Tissue slices retain much of the microenvironment as *in vivo,* such as the composition of neighboring cells and supporting structure. With abilities like nutrient refreshment and temperature control, some physiological conditions can be mimicked with a perfusion system without the confounding factors of other organs or anatomical limits[25].

Brain tissue fragility

Fresh brain tissue is notoriously difficult to maintain alive[33] and requires special equipment and delicate handling practices. Brain tissue can be cultured and maintained in media known as artificial cerebral spinal fluid, or aCSF[34]. The electrophysiology community also

commonly slice brain tissue in modified aCSF media with the addition of sucrose as a protective agent[35], as well as with reduced calcium ions to preserve neuronal membrane potential[36]. The brain slices also need to constantly be in O_2 saturated media due to its typically high O_2 demands. Although successful HP ^{13}C *ex vivo* tissue slice experiments using an NMR compatible perfusion system have been documented[37], viability of fresh brain slices in such an environment is of concern and must be tested.

Tissue viability

There are many methods for measuring tissue viability, most of which include staining. Trypan blue (TB) and LDH activity staining are popular, and operate on the reasonable assumption that damaged cell membranes leak vital components and are nonviable[38]. This assumption becomes an issue for tissue slices however, since mechanical damage to the tissue slice surfaces are inevitable. Though the surfaces are damaged, viability is not necessarily compromised in deeper layers of tissue slices. A sensible solution to measuring brain tissue slice viability is to record O_2 consumption. Brain tissue metabolism utilizes O_2 at an extreme rate[39], and any nonviable slices should exhibit a drastically reduced O_2 consumption.

The Oxygraph system (Hansatech Instruments), a variation of the Clark electrode[40], employs a platinum cathode and silver anode to measure the dissociation of an electrolyte in the presence of O_2. The electrode probes a thin membrane saturated in KCl electrolyte, of which is in contact with media in a sealed, temperature controlled chamber. The voltage recorded is directly proportional to the O_2 content in the media. Upon introduction of a viable sample, existing O_2 in media is consumed over time, and the rates can be compared. Here,

brain tissue slices are incubated within the perfusion system, and the desired outcome is to maintain viable slices for the time of a typical HP ^{13}C MRS study (<<7 hours).

Materials and methods

Animal and preparation

A 6-month-old female wild type CWT strain mouse was deeply anesthetized with 3% Isoflurane and O_2 mixture. A negative pedal pain reflex was obtained before decapitation. The fresh brain was extracted from the skull within 3 minutes of decapitation, and the cerebellum was quickly dissected and discarded. All handling practices were in accordance with University of California, San Francisco IACUC approved guidelines.

Chemicals and media

600mL of 'slicing and recovery' artificial cerebral spinal fluid ($aCSF_{recovery}$) solution was prepared with (in mM): 87 NaCl, 2.5 KCl, 25 d-glucose, 25 $NaHCO_3$, 3 $MgCl_2$, 1.25 NaH_2PO_4, 0.5 $CaCl_2$, and 75 sucrose in ddH_2O[41]. 300mL of 'typical' artificial cerebral spinal fluid (aCSF) was also prepared with (in mM): 125 NaCl, 2.5 KCl, 15 d-glucose, 26 $NaHCO_3$, 1 $MgCl_2$, 1.25 NaH_2PO_4, and 2 $CaCl_2$ in 90/10 v/v ddH_2O/D_2O[42]. All compounds are anhydrous, with exception of NaH_2PO_4 dihydrate. A 95%/5% O_2/CO_2 USP carbogen mixture (Airgas) was used to bubble into the media to satisfy the demanding O_2 requirements of brain tissue. 3% low gelling point agarose solution was prepared with 1.2g of low gelling point agarose (Sigma) and 40mL of 1M phosphate buffered saline (Thermofisher). 1.5% agarose solution was prepared with 750mg of agarose and 50mL of 1M PBS.

Tissue slicing and handling

A 3% low gelling point agarose solution was prepared and incubated at 40°C. During transfer of the incubated agarose (~5-10 seconds) through typical room temperature, the agarose cooled to 37°C and the fresh brain minus cerebellum was smothered. The entire sample was then cooled to 4°C to set the agarose. Once embedded, brain tissue was sliced to 350µm thick using the Compresstome VF-300-0Z vibrating microtome (Precisionary Instruments), and the slices bathed in a slushy 4°C $aCSF_{recovery}$ bubbled with carbogen. Taking care not to traumatize the slices, the agarose was carefully removed and the slices transferred to a carbogen-bubbled $aCSF_{recovery}$ solution incubated in a 32°C water bath. Upon slicing completion (~30 minutes), the slices were transferred to a room temperature carbogen-saturated $aCSF_{recovery}$ solution for 30 minutes.

A 50mL aliquot of aCSF was taken and was never saturated with carbogen. After the 30-minute incubation at room temperature in $aCSF_{recovery}$, a slice originating from the center brain was taken and rinsed in 15mL of unsaturated aCSF and subsequently processed in the Oxygraph. The remaining slices were placed in a 10mm NMR tube like the one established in other perfusion system studies, and was perfused with carbogen-saturated aCSF. Every hour hereafter the perfusion was stopped and a brain slice of similar size was extracted by a 5mL serological pipette with a cut tip. The slice was subsequently rinsed in the 15mL unsaturated aCSF for 1 minute and then processed in the Oxygraph. A negative control was prepared by incubating a slice in 70% ethanol at room temperature for 1 hour, and then rested in unsaturated room temperature aCSF for another hour. A slice's wet weight was recorded taking

care to aspirate as much media away as possible. The dry weight was also recorded after leaving the sample in a chemical fume hood operating at 400 CFM for 3 hours.

NMR compatible perfusion system

The perfusion system consists of a water bath, media reservoir, peristaltic pump, 10mm NMR tube, and polyethylene and silastic tubing. As illustrated in **Figure 5**, samples are placed in the NMR tube and nutrient-rich media is continuously pumped into the sample volume while 'used' media is recycled out back into the media reservoir. A 1.5% agarose plug was formed at the bottom curvature of the NMR tube to raise the slices onto a level surface. In conjunction with the pump speed, the tube lengths and diameters are set up such that a 5mL/min perfusion rate is achieved. The inflow line into the NMR tube consisted of rigid polyethylene tubing to minimize variations in flow rate. All other tubing made use of silastic due its low cost.

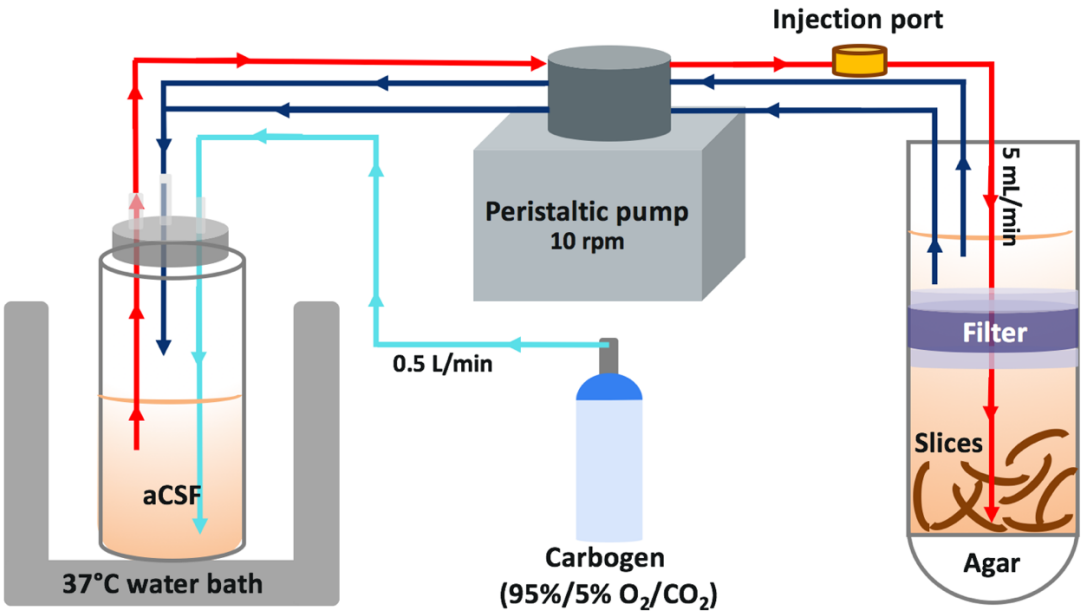

Figure 5. Illustration of perfusion system. Peristaltic pump operating at 10 rpm simultaneously drew media from reservoir sitting in 37°C into NMR tube as well as pulled media from sample tube into reservoir. Approximately 250mL of aCSF media was circulated while 95%/5% O_2/CO_2 mixture was pumped into reservoir bottle at 0.5L/min. A 1.5% agarose in PBS plug was used to raise brain slices above the curved bottom of NMR tube. A luer lock port on the inflow line was included for HP ^{13}C probe injection. Effective perfusion rate in NMR tube was 5mL/min.

Oxygen monitoring

The Oxygraph system was utilized to monitor O_2 levels of the media in the reaction chamber. The system was first calibrated by adding 2mL of ddH_2O, and the voltage was corroborated with the software's a priori knowledge of known O_2 levels in water. A zero O_2 voltage level was then achieved by introducing N_2 gas into the reaction chamber until steady state is reached. Since the electrode will pick up voltage from the electronics, the zero O_2 measurement serves as an offset correction for an accurate O_2 concentration readout. When processing a brain slice, each slice was rinsed in unsaturated aCSF media prior to measurement. A consistent 2mL of unsaturated aCSF was used in the reaction chamber, and the gas-tight plunger was replaced as quickly as possible. The spinner was set to 100%, and the water jacket temperature was calibrated to 37°C.

Results

In total 7 brain slices were measured with the Oxygraph over a period of 8 hours. **Figure 6** showcases the O_2 concentrations over time for each brain slice, as well as two media-only measurements. The different rates of O_2 consumption represent relative differences in oxidative phosphorylation activity due to time, tissue mass, and slice origin and composition. The two media measurements show a downward trend, and the negative control brain slice is within similar range.

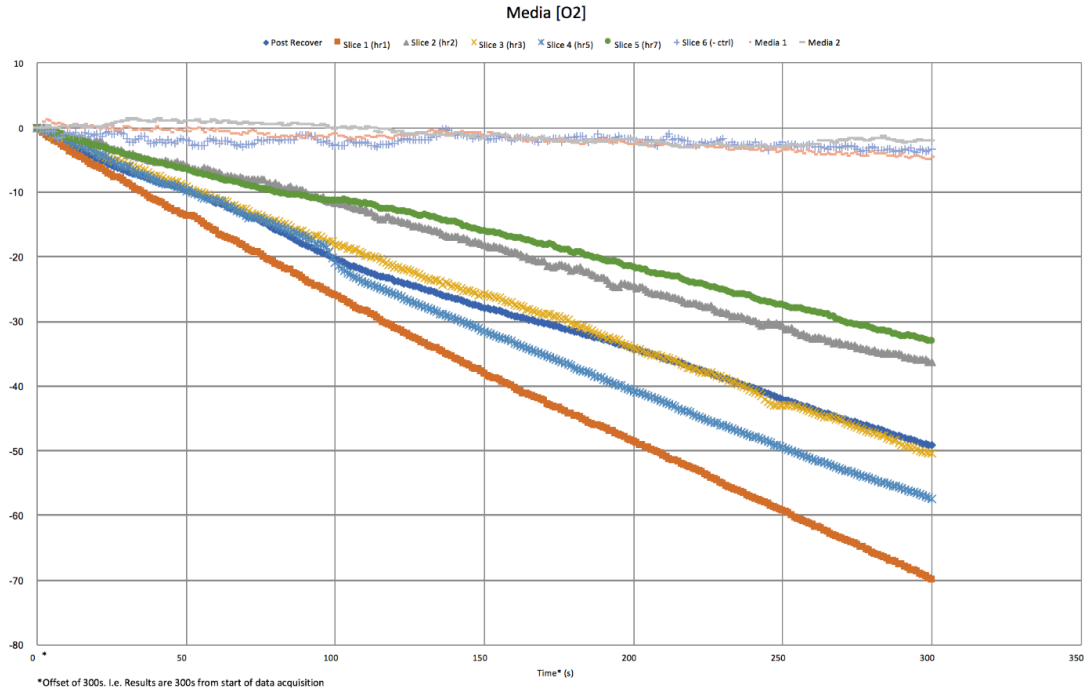

Figure 6. O_2 concentration of media in Oxygraph reaction chamber from 5-10 minutes of sample introduction. Data set to zero by subtracting each measurement's respective value at 5 minutes. Negative control exhibits similar values and decay rate compared to both media characterizations

Viability of brain tissue slices in the perfusion system over time is represented in **Figure 7**. The slice that was in the perfusion system for a single hour demonstrated the highest O_2 consumption rate, and is considered 100% viable. All other slices were compared to the slice at hour 1, reflected in their percent viability. The negative control slice's O_2 rate was 2.65% that of

slice at hour 1, and any rates near, at or below 2.65% is considered nonviable. The wet weight of a sample slice was 25mg, and the dry weight was 5.1mg.

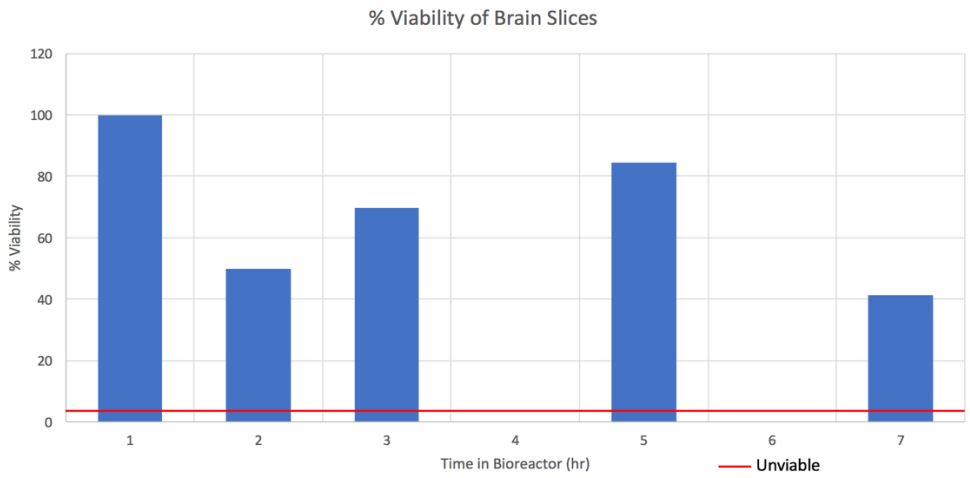

Figure 7. Percent viability of each slice at different hours from perfusion system. All values are compared to tissue slice at hour 1, and negative control measurement shown as red line.

Discussion

Oxygraph calibration and media characterization

The initial calibration of the Oxygraph was done with 2mL of ddH_2O since the software's a priori knowledge of O_2 concentration was that of water. The aCSF media used during actual measurements however contains salts and sugars that can affect the ability of retaining dissolved O_2. Thus, the absolute O_2 concentration values should not be trusted as true values, and only the slopes should be used as relative comparisons. To solve this, future work should have initial calibration with media. The two media characterization measurements were performed due to the worry that the electrode consumes a not inconsequential amount of O_2 through time. This natural O_2 decrease can be characterized with blank media measurements, and the values used for correction. The characterizations were performed at the very end of the

study however, and future work should consider media characterization throughout viability measurements.

Tissue slice selection

Care was taken to extract the tissue slices from the same position in the NMR tube for the measurements. This is difficult however, as the slices quickly agitate once the pipette was inserted for aspiration. The chosen slice as a result could have originated anywhere from the highly-perfused surface, or from the dense center mass of settled slices. This can confound the data, as slices from center mass are expected to have different viability to that of surface slices. The different positions effectively create two groups and cannot be directly compared in our context. Future work with this viability testing setup would require a more precise method of tissue extraction from the narrow NMR tube.

Normalization

The tissue slices were selected to have a similar size as to the weighed tissue. This is extremely rough however, and the unexpected nonsequential decrease in tissue viability could be attributed to this. Different masses of tissue will have a directly proportional difference in O_2 consumption. Since the slices are homogenously mixed and destroyed in the reaction chamber, tissue weighing is not an option. Normalization must be performed however, and a Bradford protein quantification assay is proposed for future work. Since the volume of media used in the Oxygraph reaction chamber is consistent, the concentration of protein can be accurately determined and used for normalization.

Chapter 3

Enzyme activity assay

Introduction

Enzyme activity assays

Enzyme activity assays are the current gold standard for studying metabolism *ex vivo*, as they are direct measurements of endogenous enzyme activity. An inclusion of activity assay data into metabolic studies of higher biological order can increase that study's robustness. Widely-used assays can also be utilized for validation of enzyme activity, due to their typically high specificity and minimal confounding variables[43]. Assays are also cost-effective, as measurements are typically performed with 96-well microplate arrays that accommodate multiple samples at a time. The goal here is to optimize sample dilutions and substrate concentrations such that the measurements are practical and within hardware capabilities.

Spectrophotometry and the NADH cofactor

Spectrophotometry is a commonly used method for determining the quantity of a chemical substance. In an enclosed environment that is impervious to external light, a light beam of similar wavelength to the target chemical's absorbance wavelength is passed through the sample. A photometer detects the amount of light that does pass through, and the difference is a direct measurement of the target chemical's abundance[44]. By measuring the abundance of a chemical through time, a rate of formation or destruction can be calculated.

In the context of LDH and PDH enzyme activities, NADH is a critical cofactor[16]. Conveniently, NADH exhibits a yellowish tint, with protocols commonly using its optimal absorbance value at a wavelength of λ = 340nm[45]. In its oxidized form, NAD^+ exhibits a different absorbance wavelength, and the spectrophotometer will consequently detect a change in NADH as the enzyme is active. When measured over time, the rate of NADH change can be used to model the target enzyme's activity.

Bradford protein quantification assay

Different samples can have different quantities of endogenous enzyme, impacting rates. Thus, all enzyme activity assays must be normalized to protein quantity, achieved through a Bradford protein quantification assay[46]. The Coomassie Blue dye is initially light brown in color, and progressively turns blue as it binds to proteins[47]. The sample is run through a spectrophotometer and compared to a known standard of protein concentrations of bovine serum albumin (BSA). The values are a direct measurement of protein quantity, and can be utilized for normalization.

Michaelis-Menten enzyme kinetics

Simple enzyme kinetics are commonly modeled by the Michaelis – Menten mechanism, originally authored by Viktor Henri[48]. Enzyme activity is characterized by the maximum conversion rate, Vmax, and the Michaelis – Menten constant, Km[49]. These values can be easily extrapolated from a Lineweaver – Burke plot[50], illustrated in **Figure 8**. The advantage to the

double-reciprocal plot is that it uses 1/absorbance vs. 1/[substrate] – both which are easily obtained from an enzyme activity assay.

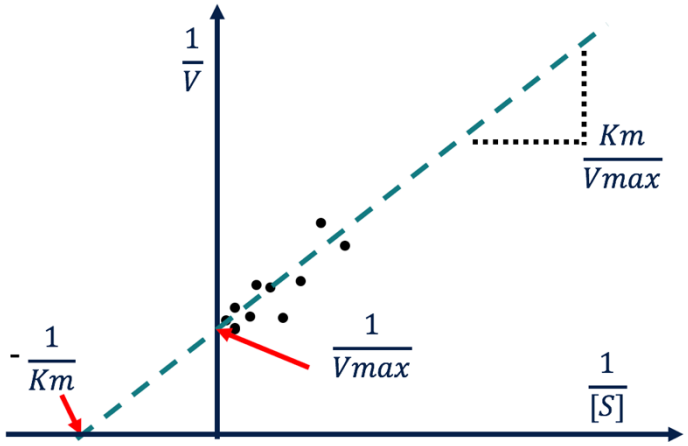

Figure 8. Lineweaver – Burke plot illustrating how enzyme activity characteristics are extrapolated.

Materials and methods

Animal and preparation

A fresh hippocampal brain section was pre-prepared from C57BL/6J strain control mice and stored at -80°C. The 21.2mg tissue sample was diluted with 400µL of 1M PBS in a Dounce homogenizer. Roughly 20-30 passes were performed over ice to ensure complete homogenization while minimizing heat degradation. Approximately 350µL of homogenate was successfully aspirated and deposited into an Eppendorf tube. Dilutions 52, 10, and 20 were prepared for Bradford, PDH, and LDH assays, respectfully.

Chemicals

A PDH enzyme activity microplate assay kit (abcam) was used to measure PDH activity. For LDH activity assays, a reaction buffer was prepared with 80mM Tris and 200mM NaCl adjusted to a pH of 7. A gradient of pyruvate concentrations was also created by first preparing

a 100mM sodium pyruvate stock, and mixed with the reaction buffer to achieve desired concentrations as seen in **Table 3a**. A 6mM NADH stock was prepared by adding 5mg of NADH (Research Products International) to 1.175mL of reaction buffer, and an NADH standard created by mixing the stock with reaction buffer to achieve desired concentrations as seen in **Table 3b**. An initial 32μg/50μL BSA concentration was prepared by adding 425μL of 1M PBS to 200μL of 2mg/mL Albumin standard (Thermofisher). Serial dilutions in 1M PBS were performed to create the Bradford standard, ending with a 0.5μg/50μL concentration. Coomassie blue G-250 dye (Thermofisher) stored at 4°C was used as is.

a

[Pyr] (mM)	0.5	1	1.5	2	2.5	3	5	8
Pyr stock (μL)	30	60	90	120	150	180	300	480
Rxn buffer (μL)	5970	5940	5910	5880	5850	5820	5700	5520
Total (μL)	6000	6000	6000	6000	6000	6000	6000	6000

b

NADH (nmol)	0	7.5	15	22.5	30	37.5
NADH stock (μL)	0	5	10	15	20	25
Rxn buffer (μL)	600	595	590	585	580	575
Total (μL)	600	600	600	600	600	600

Table 3. Concentrations of solutions used for LDH assay. (a) Pyruvate concentration gradient prepared with varying volumes of 100mM pyruvate stock in reaction buffer. (b) NADH standard gradient formed with 6mM NADH stock in reaction buffer.

Bradford protein quantification assay

5μL of dilution 52 sample was plated on a 96-well clear flat bottom microplate in triplicate. For the standard, 5μL of each BSA concentration were plated in duplicate. Two wells were filled with 5μL of blank 1M PBS to measure background. 100μL of Coomassie blue was pipetted into every well in use. The microplate was covered in foil and incubated at 37°C for 30

minutes before measurement. The wavelength absorbance for Coomassie blue was set to 595nm. All assays were read with the Infinite M200 (Tecan) spectrophotometer.

PDH activity assay

200μL of dilution 10 sample was loaded in duplicate onto the kit's antibody-coated microplate. A background well loaded with 200μL of the kit's sample buffer was included for offset correction. The kit's protocol was carefully followed, and the microplate was read with the spectrophotometer set to 450nm. The data was acquired over 45 minutes at an interval of 1 minute.

LDH activity assay

In a clean 96-well microplate, 5μL of dilution 20 sample was loaded in triplicate for 8 rows to ensure all 8 concentrations of pyruvate solution were utilized. The 6mM NADH stock was added to each of the pyruvate concentrations such that a final 0.2mM concentration of NADH per well was achieved. 150μL of each NADH standard concentration was loaded. The spectrophotometer absorbance was set to 340nm, and the pyruvate – NADH mixtures were added once everything was ready. The measurements were taken in every 2 minute intervals for a total of 30 minutes.

Calculation and analysis

For PDH activity, the absorbance (OD) between 4 minutes and 24 minutes were considered in the slope calculation. The rate was normalized to protein concentration

determined by the Bradford assay results, and the values of duplicates were averaged. For LDH, the slope between minutes 2 and 14 were considered. The values of triplicates were compared, and any outlier slopes were excluded before averaging. The NADH/min was calculated by dividing the absorbance slope by the change in absorbance observed from the NADH standard. The value was also normalized to protein concentration. The Km was calculated by dividing the slope of Lineweaver – Burke by the y-intercept. Vmax is calculated by taking the reciprocal of the y-intercept.

Results

PDH activity after correcting for protein concentration was 5.27 OD/min/[P]. The absorbance over time is shown in **Figure 9**. The Lineweaver – Burke plot for LDH activity assay is displayed in **Figure 10.** After correcting for protein concentration, Km is 0.4mM and Vmax is 41.13μM/min/[P].

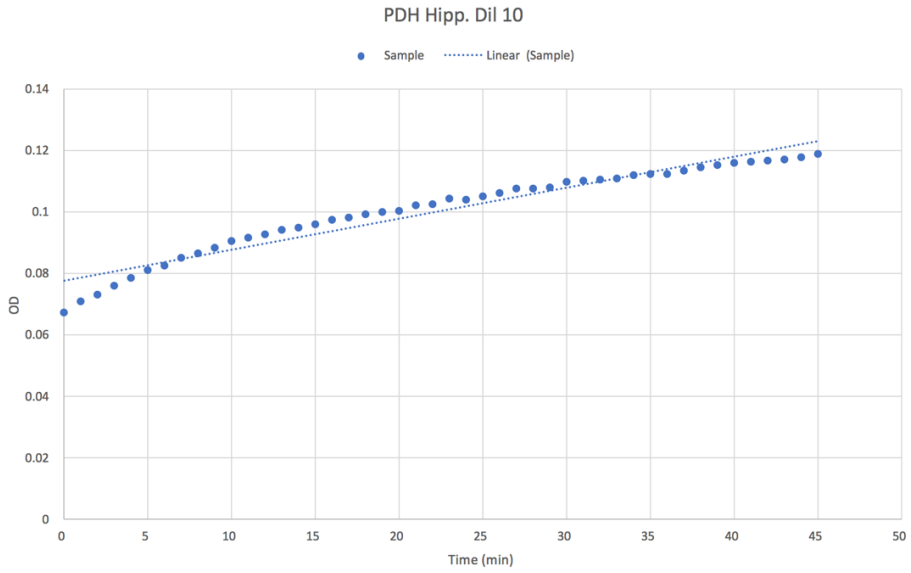

Figure 9. Absorbance over time for PDH activity assay.

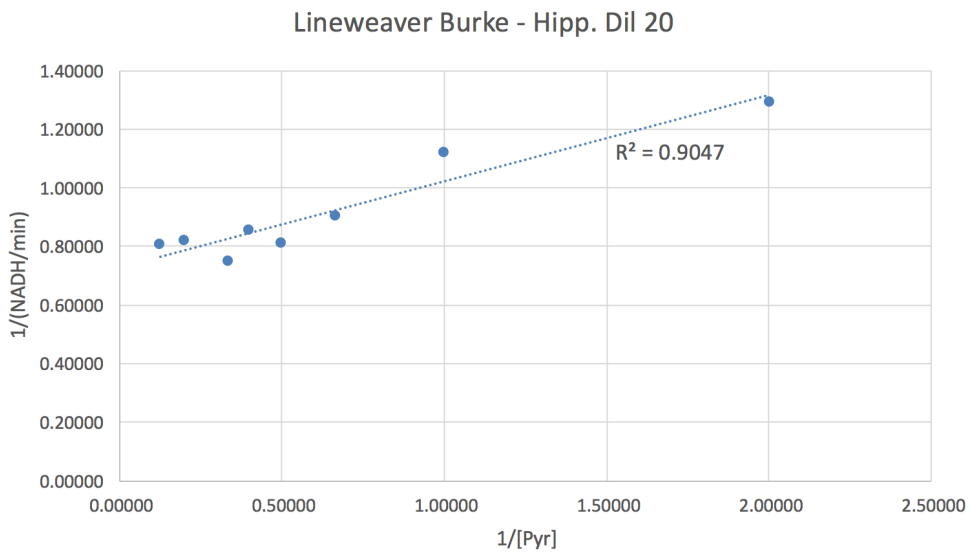

Figure 10. Lineweaver – Burke plot with eight different concentrations of pyruvate.

Discussion

The sample dilutions and substrate concentrations employed for the PDH and LDH assays were optimal. A too low of a dilution would saturate the signal and render the dynamic assay useless. A too high of a dilution could wash out the activity, as the main inhibitor would be a low enzyme to substrate ratio. Optimal dilutions and substrate concentrations produce an OD curve that's linear for at least 10 minutes, as demonstrated in **Figure 9**. The linearity achieved here incorporates more data points, allowing for accurate determination of NADH oxidation and reduction rates. Although only an N = 1, reproducibility should not be an issue given the high intrinsic sensitivity of the method, and future work includes optimizing dilutions for a wide range of tissue masses.

Chapter 4

General Discussion

3-component system

In vivo HP ^{13}C MRS

In vivo imaging studies are highly translatable to the clinic, with the major goal of satisfying unmet needs. Preclinical HP ^{13}C MRS characterization of neuroinflammation and trauma[31] exist, with more disease models emerging. With [1-^{13}C] pyruvate, lactate and bicarbonate peaks are important since they are strong indicators of LDH and PDH enzyme activity, respectively. Bicarbonate is naturally difficult to observe however, since it is formed after a second catalysis[16] from pyruvate. Methodology is quickly advancing though, such as the development of selective excitation pulse sequences[30] and proton decoupling[9]. These methods were not employed here however, as the in-house developed coil's sensitivity to bicarbonate was still in question, and was tested here with a basic pulse acquire sequence.

Ex vivo NMR compatible perfusion system

The use of an NMR compatible perfusion system for fresh brain tissue slices is extremely rare, with only a single documentation published just three months prior of this writing[42]. The concept is extremely powerful though, since it is the closest to providing near absolute metabolic rates of very specific targets in a physiological environment. Combined with the strength of HP ^{13}C, this second component of the system will provide crucial data and add robustness to *in vivo* studies. The concern of maintaining brain slice viability was addressed

here, but future work includes addition of normalization and testing reproducibility. An actual HP ^{13}C MRS study also yet to be performed, and is currently planned.

Enzyme activity

The enzyme activity assays are arguably unnecessary, but are relatively cheap and quick methods that drastically add to the robustness of a study. Activity assays are still considered the gold standard for studying metabolism, and so should be included as a validation tool.

Future work

There is much work to be done, including optimizing sequences and reproducing data for *in vivo* imaging, reproducible viability tests and HP ^{13}C MRS study for *ex vivo* perfusion system, and an expanded optimization for different tissue masses when running enzyme activity assays. The 3-component system is intended to run paired studies, where one subject is probed by all the methods. A major future milestone is to assess the success of such a trial.

Conclusion

The 3-component system of studying brain metabolism with HP ^{13}C MRS is designed such that a single component's flaws are covered by the other components' strengths. For an ideal study in an ideal world, every method fathomable would be used for one hypothesis. This is impractical however, as time and resources are limited. The 3 components promoted here already span a large field in biology and engineering, and are suitable for answering most metabolic study questions on a wide range of mouse models.

References

1. Nambron R, Silajdžić E, Kalliolia E, et al. A Metabolic Study of Huntington's Disease. Eckel J, ed. *PLoS ONE*. 2016;11(1):e0146480.
2. Craft S. The Role of Metabolic Disorders in Alzheimer's Disease and Vascular Dementia: Two Roads Converged? *Archives of neurology*. 2009;66(3):300-305.
3. Pathak D, Berthet A, Nakamura K. Energy Failure: Does It Contribute to Neurodegeneration? *Ann Neurol*. 2013;74:506-516.
4. Prabakaran S, Swatton JE, Ryan MM, Huffaker SJ, et al. Mitochondrial dysfunction in schizophrenia: evidence for compromised brain metabolism and oxidative stress. *Molecular Psychiatry.* 2004;9:684-697.
5. Rubinstein M, Shiffman S, Moscicki A, et al. Nicotine metabolism and addiction among adolescent smokers. *Addiction.* 2013;108(2):406-12.
6. Yoon BK, Kim J. How to Begin Molecular Research of Metabolic Diseases. *Endocrinology and Metabolism*. 2016;31(4):505-509.
7. Tognarelli JM, Dawood M, Shariff MIF, et al. Magnetic Resonance Spectroscopy: Principles and Techniques: Lessons for Clinicians. Journal of Clinical and Experimental Hepatology. 2015;5(4):320-328.
8. Gruetter R, Adriany G, Choi I-Y, Henry P-G, Lei H, Öz G. Localized *in vivo* ^{13}C NMR spectroscopy of the brain. *NMR in biomedicine*. 2003;16(6-7):313-338.
9. Kurhanewicz J, Bok R, Nelson SJ, Vigneron DB. Current and Potential Applications of Clinical ^{13}C MR Spectroscopy. *Journal of nuclear medicine: official publication, Society of Nuclear Medicine*. 2008;49(3):341-344.
10. Brandes AH, Ward CS, Ronen SM. 17-Allyamino- 17-demethoxygeldanamycin treatment results in a magnetic resonance spectroscopy-detectable elevation in choline-containing metabolites associated with increased expression of choline transporter SLC44A1 and phospholipase A2. *Breast Cancer Research*. 2010;12(5):R84.
11. de Graaf RA, Mason GF, Patel AB, Behar KL, Rothman DL. In vivo 1H-[13C]-NMR spectroscopy of cerebral metabolism. *NMR Biomed.* 2003;16(6-7):339-57
12. Ardenkjaer-Larsen JH, Fridlund B, Gram A, Hansson G, et al. Increase in signal-to-noise ratio of >10,000 times in liquid-state NMR. *Proceedings of the National Academy of Sciences of the United States of America*. 2003;100(18):10158-163.
13. Chaumeil MM, Najac C, Ronen SM. Studies of Metabolism using ^{13}C MRS of Hyperpolarized Probes. *Methods Enzymol.* 2015;561:1-71.
14. Koelsch BL, Keshari KR, Peeters TH, Larson PE, Wilson DM, Kurhanewicz J. Diffusion MR of hyperpolarized 13C molecules in solution. *Analyst*. 2013b;138(4):1011–1014.
15. Wilson DM, Keshari KR, Larson PE, Chen AP, Hu S, Van Criekinge M, et al. Multi-compound polarization by DNP allows simultaneous assessment of multiple enzymatic activities in vivo. *Journal of Magnetic Resonance* 2010;205(1):141–147.
16. Nelson DL, Cox MM. Lehninger Principles of Biochemistry. 6th edition. New York: W H Freeman; 2013. p. 541-634

17. Berg JM, Tymoczko JL, Stryer L. Biochemistry. 5th edition. New York: W H Freeman; 2002. Chapter 17, The Citric Acid Cycle.

18. Albers MJ, Bok R, Chen AP, Cunningham CH, Zierhut ML, Zhang VY, et al. Hyperpolarized ^{13}C lactate, pyruvate, and alanine: Noninvasive biomarkers for prostate cancer detection and grading. *Cancer Research*. 2008;68(20):8607–8615.

19. Larson PE, Bok R, Kerr AB, Lustig M, Hu S, Chen AP, et al. Investi- gation of tumor hyperpolarized [1-13C]-pyruvate dynamics using time-resolved multiband RF excitation echo-planar MRSI. *Magnetic Resonance in Medicine*. 2010;63(3):582–591.

20. Keshari KR, Wilson DM, Chen AP, Bok R, Larson PE, Hu S, et al. Hyperpolarized [2-13C]-fructose: A hemiketal DNP substrate for in vivo metabolic imaging. *Journal of the American Chemical Society.* 2009;131(48):17591–17596.

21. Schroeder MA, Cochlin LE, Heather LC, Clarke K, Radda GK, Tyler DJ. *In vivo* assessment of pyruvate dehydrogenase flux in the heart using hyperpolarized carbon-13 magnetic resonance. *PNAS*. 2008;105(33):12051-12056.

22. Park I, Larson PE, Zierhut ML, Hu S, Bok R, Ozawa T, et al. Hyperpolarized 13C magnetic resonance metabolic imaging: Application to brain tumors. *Neuro-Oncology*. 2010;12(2):133–144.

23. Nelson SJ, Kurhanewicz J, Vigneron DB, et al. Metabolic Imaging of Patients with Prostate Cancer Using Hyperpolarized [1-^{13}C]Pyruvate. *Science translational medicine*. 2013;5(198):198ra108.

24. Chaumeil MM, Radoul M, Najac C, et al. Hyperpolarized 13C MR imaging detects no lactate production in mutant IDH1 gliomas: Implications for diagnosis and response monitoring. *Neuroimage Clin.* 2016;12:180-189.

25. Pysz MA, Gambhir SS, Willmann JK. Molecular Imaging: Current Status and Emerging Strategies. *Clinical radiology*. 2010;65(7):500-516.

26. Scarfe L, Brillant N, Kumar JD, Ali N, Alrumayh A, et al. Preclinical imaging methods for assessing the safety and efficacy of regenerative medicine therapies. *npj Regenerative Medicine*. 2017;2(28).

27. Von Morze C, Bok RA, Reed GD, Ardenkjaer-Larsen JH, Kurhanewicz J, Vigneron DB. Simultaneous Multiagent Hyperpolarized 13C Perfusion Imaging. *Magnetic resonance in medicine: official journal of the Society of Magnetic Resonance in Medicine / Society of Magnetic Resonance in Medicine*. 2014;72(6):1599-1609.

28. Naressi A, Couturier C, Devos JM, Janssen M, Mangeat C, de Beer R, Graveron-Demilly D. Java-based Graphical User Interface for the MRUI Quantitation Package. *MAGMA*. 2001;12:141-152.

29. Vanhamme L, van den Boogaart A, Van Huffel S. Improved method for accurate and efficient quantification of MRS data with use of prior knowledge. *Journal of Magnetic Resonance*. 1997;129:35-43.

30. Von Morze C, Sukumar S, Reed GD, et al. Frequency-specific SSFP for hyperpolarized ^{13}C metabolic imaging at 14.1T. *Magnetic Resonance Imaging*. 2013;31(2):10.1016/j.mri.2012.06.037.

31. Marjańska M, Iltis I, Shestov AA, et al. In Vivo13C Spectroscopy in the Rat Brain using Hyperpolarized [1-13C]pyruvate and [2-13C]pyruvate. *Journal of magnetic resonance*. 2010;206(2):210-218.

32. Guglielmetti C, Chou A, Krukowski K, et al. In vivo metabolic imaging of Traumatic Brain Injury. *Scientific Reports*. 2017;7:17525.

33. Ting JT, Daigle TL, Chen Q, Feng G. Acute brain slice methods for adult and aging animals: application of targeted patch clampanalysis and optogenetics. *Methods in molecular biology*. 2014;1183:221-242

34. An JH, Su Y, Radman T, Bikson M. Effects of glucose and glutamine concentration in the formulation of the artificial cerebrospinal fluid (ACSF). *Brain research*. 2008;1218:77-86.

35. Moyer JR, Jr, Brown TH. Methods for whole-cell recording from visually preselected neurons of perirhinal cortex in brain slices from young and aging rats. *J Neurosci Meth*. 1998;86:35–54.

36. Kim S, Ma L, Yu CR. Requirement of calcium-activated chloride channels in the activation of mouse vomeronasal neurons. *Nature Communications*. 2011;2:365.

37. Keshari KR, Sriram R, Van Criekinge M, et al. Metabolic Reprogramming and Validation of Hyperpolarized ^{13}C Lactate as a Prostate Cancer Biomarker Using a Human Prostate Tissue Slice Culture Bioreactor. *Prostate*. 2013;73(11):1171-1181.

38. Gantenbein-Ritter B, Potier E, Zeiter S, van der Werf M, Sprecher CM, Ito K. Accuracy of Three Techniques to Determine Cell Viability in 3D Tissues or Scaffolds. *Tissue Engineering*. 2008;14(4):353-358.

39. Hall CN, Klein-Flügge MC, Howarth C, Attwell D. Oxidative phosphorylation, not glycolysis, powers pre- and postsynaptic mechanisms underlying brain information processing. *The Journal of neuroscience: the official journal of the Society for Neuroscience*. 2012;32(26):8940-8951.

40. Clark LC Jr. Monitor and control of blood and tissue oxygen tension. *Trans. Am. Soc. artif. internal Organs. 1956;*2:41.

41. Murata A, Agematsu K, Korotcova L, Gallo V, Jonas RA, Ishibashi N. Rodent Brain Slice Model for the Study of White Matter Injury. *The Journal of thoracic and cardiovascular surgery*. 2013;146(6):10.1016/j.jtcvs.2013.02.071.

42. Harris T, Azar A, Sapir G, et al. Real-time *ex-vivo* measurement of brain metabolism using hyperpolarized [1-^{13}C]pyruvate. *Scientific Reports.* 2018;8:9564.

43. Sancenon V, Goh WH, Sundaram A, Er KS, Johal N, et al. Development, validation, and quantitative assessment of an enzymatic assay suitable for small molecule screening and profiling: A case study. *Biomolecular Detection and Quantification*. 2015;4:1-9.

44. Gore M. Spectrophotometry & Spectrofluorimetry. New York: Oxford University Press, 2000.

45. Held P. Determination of NADH Concentrations with Synergy™ 2 Multi-Detection Microplate Reader using Fluorescence or Absorbance. *BioTek Instruments*. 2007.

46. Ernst O, Zor T. Linearization of the Bradford Protein Assay. Journal of Visualized Experiments: *JoVE*. 2010;(38):1918.

47. Congdon RW, Muth GW, Splittgerber AG. The Binding Interaction of Coomassie Blue with Proteins. *Analytical Biochemistry*. 1993;213(2):407-413.

48. Schnell S, Chappell MJ, Evans ND, Roussel MR. The mechanism distinguishability problem in biochemical kinetics: The single-enzyme, single-substrate reaction as a case study. *Comptes Rendus Biologies*. 2006;329(1):51-61.

49. Schnell S, Maini PK. A Century of Enzyme Kinetics: Reliability of K_m and v_{max} Estimates. *Theoretical Biology*. 2003;8:169-187.

50. Berg JM, Tymoczko JL, Stryer L. Biochemistry. 5th edition. New York: W H Freeman; 2002. Appendix: Vmax and KM Can Be Determined by Double-Reciprocal Plots.

Publishing Agreement

It is the policy of the University to encourage the distribution of all theses, dissertations, and manuscripts. Copies of all UCSF theses, dissertations, and manuscripts will be routed to the library via the Graduate Division. The library will make all theses, dissertations, and manuscripts accessible to the public and will preserve these to the best of their abilities, in perpetuity.

Please sign the following statement:

I hereby grant permission to the Graduate Division of the University of California, San Francisco to release copies of my thesis, dissertation, or manuscript to the Campus Library to provide access and preservation, in whole or in part, in perpetuity.

Author Signature

08/31/2018
Date